ACS Synthetic Biology
Cite This: ACS Synth. Biol. 2019, 8, 775−786
Research Article
pubs.acs.org/synthbio

Sensor-Enabled Alleviation of Product Inhibition in Chorismate Pyruvate-Lyase

Ramesh K. Jha,*[,†] Niju Narayanan,[†] Naresh Pandey,[§] Jeremy M. Bingen,[†] Theresa L. Kern,[†] Christopher W. Johnson,[‡] Charlie E. M. Strauss,[†] Gregg T. Beckham,[‡] Scott P. Hennelly,[§] and Taraka Dale*[,†]

[†]Bioscience Division, MS M888, Los Alamos National Laboratory, Los Alamos, New Mexico 87545, United States
[§]Theoretical Biology and Biophysics, Theoretical Division, Los Alamos National Laboratory, Los Alamos, New Mexico 87545, United States
[‡]National Bioenergy Center, National Renewable Energy Laboratory, Golden, Colorado 80401, United States

Supporting Information

ABSTRACT: Product inhibition is a frequent bottleneck in industrial enzymes, and testing mutations to alleviate product inhibition via traditional methods remains challenging as many variants need to be tested against multiple substrate and product concentrations. Further, traditional screening methods are conducted *in vitro*, and resulting enzyme variants may perform differently *in vivo* in the context of whole-cell metabolism and regulation. In this study, we address these two problems by establishing a high-throughput screening method to alleviate product inhibition in an industrially relevant enzyme, chorismate pyruvate-lyase (UbiC). First, we engineered a highly specific, genetically encoded biosensor for 4-hydroxybenzoate (4HB) in an industrially relevant host, *Pseudomonas putida* KT2440. We subsequently applied the biosensor to detect the activity of a heterologously expressed UbiC that converts chorismate into 4HB and pyruvate. By using benzoate as a product surrogate that inhibits UbiC without activating the biosensor, we were able to efficiently create and screen a diversified library for UbiC variants with reduced product inhibition. Introduction of the improved UbiC enzyme variant into an experimental production strain for the industrial precursor *cis,cis*-muconic acid (muconate), enabled a >2-fold yield improvement for glucose to muconate conversion when the new UbiC variant was expressed from a plasmid and a 60% yield increase when the same UbiC variant was genomically integrated into the strain. Overall, this work demonstrates that by coupling a library of enzyme variants to whole-cell catalysis and biosensing, variants with reduced product inhibition can be identified, and that this improved enzyme can result in increased titers of a downstream molecule of interest.

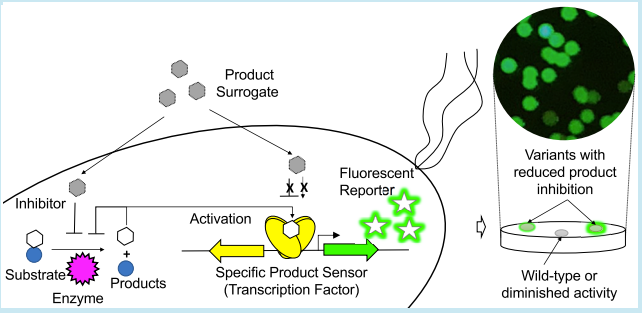

KEYWORDS: *product inhibition, biosensor, UbiC, cis,cis-muconic acid, PobR, 4-hydroxybenzoate, Pseudomonas putida KT2440*

Depleting petroleum reserves, energy security concerns, and global climate change have driven collective efforts worldwide to search for alternate technologies to transition to a biobased sustainable society.[1] Microbial biosynthesis provides a sustainable route from renewable feedstocks to the production of platform chemicals, polymer precursors, and fuels currently sourced from petroleum. The success of a biosynthetic pathway is dependent on multiple factors including the pathway genes, discovery of enzymes for non-natural metabolic pathways, promoters, choice of microbial host, availability of cofactors, enzyme activities, and stress regulons. Often, the balance between these factors is offset because of the complexities of biological systems, resulting in low product titers and yields, as well as poor cell physiology. Advances in computational tools and synthetic biology methods have enabled researchers to design and rapidly build billions of cells with varying metabolic design.[2] However, the methodologies currently available for testing the designs lag by several orders of magnitude and form a major bottleneck in the design−build−test−learn cycle for biobased products.

Biosensors have emerged as powerful tools for the rapid screening and isolation of the best combination of genetic components without their individual evaluation. A whole-cell biosensor comprising a transcription factor activation (sensor) by a metabolic intermediate or a final product coupled to fluorescence readout (reporter) has been effectively utilized to enhance enzymes[3,4] and improve the efficiency of metabolic pathways,[4−6] host strains, and overall product titers and yields.[7−9] To our knowledge, such a biosensor technology has not been applied to engineer an enzyme for alleviated product inhibition. Traditional methods to engineer enzymes with

Received: November 6, 2018
Published: March 12, 2019

DOI: 10.1021/acssynbio.8b00465
ACS Synth. Biol. 2019, 8, 775−786

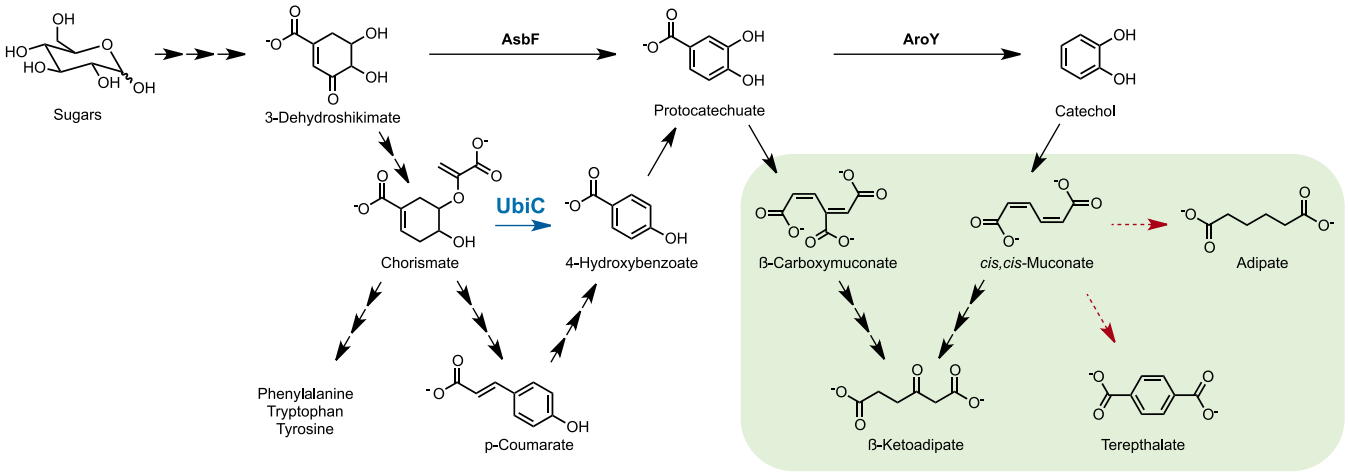

Figure 1. 4-Hydroxybenzoate (4HB) is a precursor to multiple value-added chemicals (green boxes). The reaction of interest from chorismate to 4HB catalyzed by UbiC is indicated by a single blue arrow. Chemical transformations are shown as dotted arrows. Multistep transformations are represented with multiple arrows. An alternate route leading to the value-added chemicals from the shikimate pathway via 3-dehydroshikimate to protocatechuate conversion and catalyzed by enzyme AsbF is also shown.

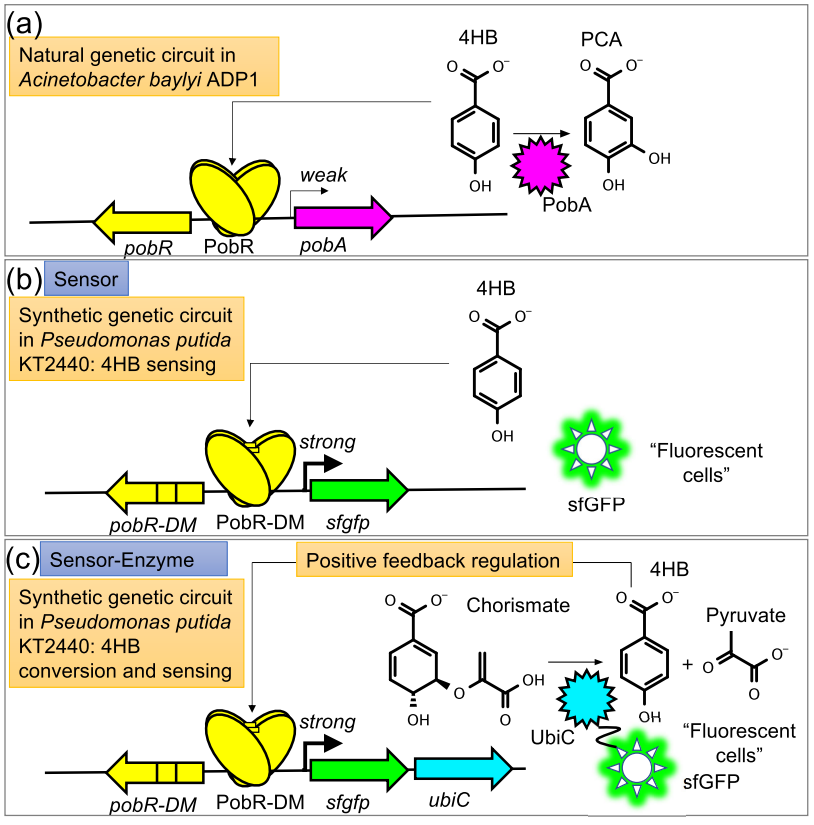

Figure 2. Natural and synthetic genetic circuits involving the PobR transcription factor (TF). (a) The natural PobR activates a promoter for expression of PobA that converts 4HB to PCA. (b) Sensor: A synthetic construct designed for 4HB sensing consisting of a double mutant of PobR (PobR-DM) that has a stronger activation of the promoter than the natural TF (depicted by a thick arrow), which results in a high expression of sfGFP (reporter). (c) Sensor-Enzyme: A synthetic construct for 4HB conversion and sensing consisting of the same PobR-DM sensor and promoter but resulting in an expression of sfGFP fused UbiC (reporter). Hence, the promoter is under positive feedback regulation of the UbiC activity, which catalyzes the conversion of chorismate into 4HB and pyruvate.

reduced product inhibition utilizing site-directed mutagenesis pose restrictions on the number of variants that can be evaluated, largely because of the need to compare each mutant against a range of concentrations of inhibitor or the product itself. Even with the use of multiwell plate-based methods, individual screening of hundreds of mutant combinations would be time-consuming and would still result in only *in vitro* data. Hence, a high-throughput, *in vivo* screening method is needed to be able to rapidly screen through a library of inhibition-relieving mutations. However, an inherent limitation of the use of a whole-cell biosensor to alleviate product inhibition arises because of the need to "sense" product formed

DOI: 10.1021/acssynbio.8b00465
ACS Synth. Biol. 2019, 8, 775−786

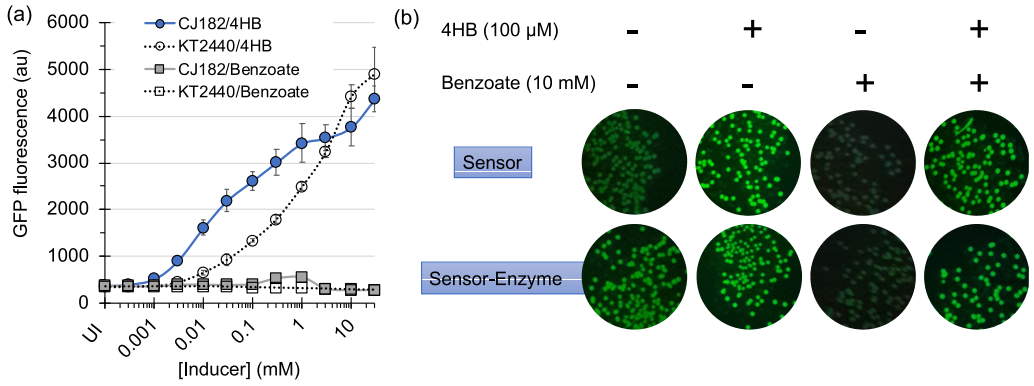

Figure 3. (a) Dose−response plot of *P. putida* strains (wild-type KT2440 and CJ182) transformed with the PobR-DM sensor plasmid (pPobR). *Y*-axis shows the mean raw fluorescence of approximately 100,000 cells. Error bars are standard deviations from duplicate experiments. UI (uninduced) fluorescence intensity numbers represent cell autofluorescence. (b) Colonies of CJ182, with the plasmid pPobR (Sensor), or with the UbiC plasmid pPobR_ubiC-wt (Sensor-Enzyme), grown in the presence or absence of 100 μM 4HB and/or 10 mM benzoate inhibitor.

while in the presence of an inhibitory concentration of product already in the experimental environment. The combination of a product surrogate that mimics the product inhibition and a highly specific biosensor (that "senses" the actual product but not the surrogate) could address this problem.

In this work, we targeted chorismate pyruvate-lyase (UbiC), which has been recognized as a potential industrial enzyme that can enable the conversion of sugars into value-added chemicals.[10,11] UbiC converts chorismate to 4-hydroxybenzoate (4HB) and pyruvate and also experiences product inhibition by 4HB, which inhibits UbiC with high affinity (K_p ~ 2 μM).[12] Although 4HB is naturally utilized as a precursor for the ubiquinone synthesis pathway,[13] it also can shunt carbon toward pathways for the production of value-added products (Figure 1). For example, this metabolic route has been demonstrated in conjunction with a shunt from dehydroshikimate (DHS) to protocatechuate (PCA) and showed an improvement in the titer and yield of *cis,cis*-muconate in *Escherichia coli*.[10] Thus, since the utility of UbiC is hampered by negative feedback regulation, any increase in the tolerance of 4HB by UbiC could enhance the production of value-added products generated via the conversion of chorismate to 4HB.

In this work, we established a 4-hydroxybenzoate (4HB) biosensor in an industrially relevant microorganism, *Pseudomonas putida* KT2440, and we used the sensor to optimize the heterologous *Escherichia coli ubiC* gene product for reduced product inhibition. In our whole-cell catalysis and sensing approach, we paired a double mutant of the PobR transcription factor (PobR-DM)[14] that showed high sensitivity and dynamic range for 4HB, with the native Pob promoter (P_{pob}) to regulate the expression of a fluorescent protein reporter in fusion with UbiC (Figure 2). Since the activity of UbiC resulted in 4HB formation and correlated PobR-DM activation, the fluorescence protein reporter was under positive feedback regulation of UbiC activity. This system was used in the presence of a product surrogate (benzoate) to screen UbiC variants for reduced product inhibition. This permitted the screening of 400 mutant variants in a single experiment. Further, we incorporated the improved enzyme into a synthetic pathway for the production of *cis,cis*-muconic acid, a renewable platform molecule and an established precursor to the building blocks of nylon-6,6,[15−18] polyethylene terephthalate,[19] and a variety of unsaturated polyesters.[20,21]

RESULTS

Double Mutant of *Acinetobacter baylyi* ADP1 PobR and Activity in *Pseudomonas putida* KT2440 for 4HB Biosensing. PobR-DM is a double mutant (ΔL141, L220V) of the native PobR transcription factor from *Acinetobacter baylyi* ADP1. When paired with the native promoter (P_{pob}) and tested in *E. coli*, the transcription factor exhibited very high sensitivity to 4HB.[14,22] The sensor also did not respond to closely related molecules like *p*-nitrophenol[22] and very weakly responds to protocatechuate, but only at 1000-fold greater concentration than the native inducer, 4HB.[14] The genetic fragment encoding PobR-DM and the promoter, along with the *sfgfp* (coding for a superfolder GFP)[23] reporter, were cloned into a broad host range pBTL-2 vector.[24] The resulting sensor plasmid, pPobR, was transformed into native *P. putida* KT2440 and CJ182, an engineered strain incapable of metabolizing 4HB due to deletion of the native *pobA*.[25] The whole-cell biosensor when grown in a regular rich medium (Lysogeny Broth) responded to 4HB in a dose-dependent manner, showed high sensitivity (lowest detection concentration <3 μM exogenous 4HB in CJ182 and <30 μM in native KT2440), and had a contrast ratio of >12-fold at 30 mM inducer concentration. In other words, for a given exogenous 4HB concentration (<3 mM), the sensor reports that there is a higher intracellular 4HB concentration in CJ182 than in the native KT2440. These results makes intuitive sense based on the genotypes of these two strains: KT2440 metabolizes 4HB, which is expected to result in a lower intracellular concentration of 4HB, while CJ182 is expected to accumulate 4HB intracellularly due to the PobA deletion. Importantly, the whole-cell biosensor did not show any response to benzoate, a molecule similar to 4HB but lacking the hydroxyl group (Figure 3a). These data confirmed that the 4HB sensor is functional, sensitive, and specific for detection of 4HB in *P. putida*.

Intracellular 4HB Production and Sensing. The *E. coli* gene that encodes for UbiC was introduced into the pPobR sensor plasmid and in the same reading frame as the *sfgfp* reporter. In this positive feedback regulation set up, the enzymatic activity of UbiC regulated its own expression as a sfGFP fusion protein: specifically, higher UbiC activity should lead to more 4HB, which in turn increases activation of the sensor, which then leads to an increase in the expression of that *ubiC* gene (Figure 2c). *P. putida* CJ182 cells showed high

DOI: 10.1021/acssynbio.8b00465
ACS Synth. Biol. 2019, 8, 775−786

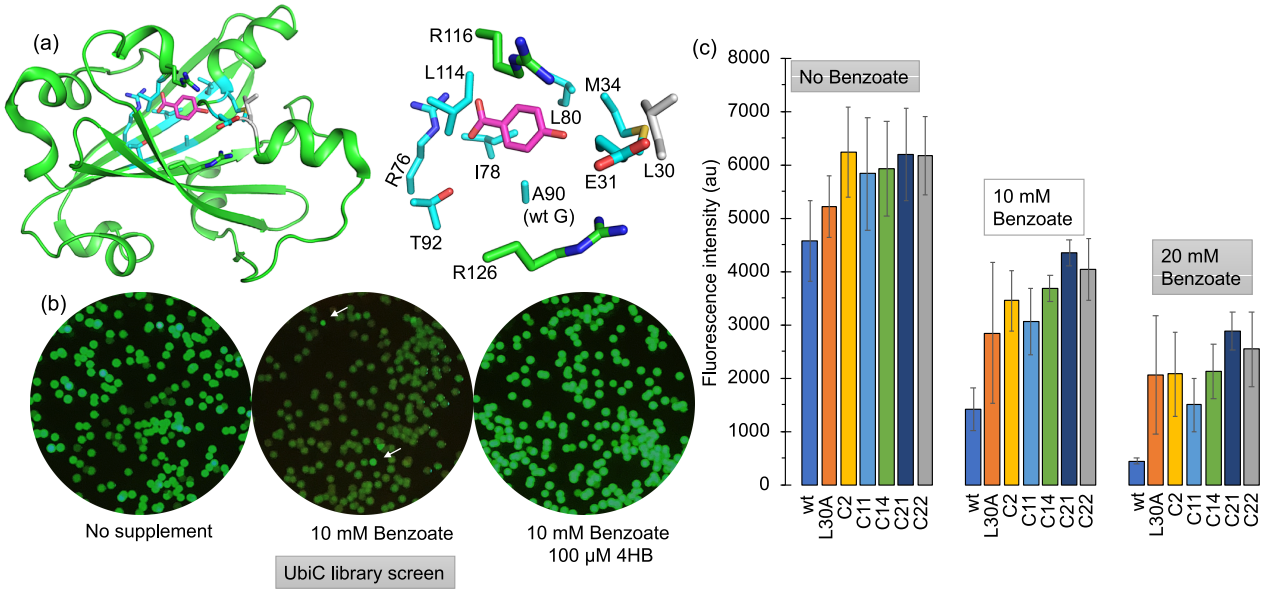

Figure 4. UbiC library and screening. (a) Structure-based selection of mutational positions in UbiC based on the product-bound structure from X-ray crystallography (PDB code 1JD3).[27] Whole protein (left) and targeted residues (right). Residues R116 and R126 (green) were not mutated, but neighboring residues (cyan) were mutated to make the "flap" (residues 29−34)[28] flexible, promoting exit of the product. M34 interacts with L30, and E31 interacts with R116 and R126. The residue numbers are based on the numbering in the published UbiC structure. Protein structures were created using PyMOL (The PyMOL Molecular Graphics System, Version 2.2, Schrödinger, LLC). (b) UbiC library plated on LB agar medium with supplementation. The colonies that were picked on the basis of the fluorescence intensity in the presence of 10 mM benzoate are marked with white arrows. Note: Only a small portion of Petri dish is shown here for clarity. Colonies from crowded regions were avoided since *P. putida* is capable of metabolizing benzoate, which would decrease the local concentration around nearby cells and artificially relieve the UbiC inhibition. (c) Quantitative evaluation of selected clones in liquid culture supplemented with different concentrations of benzoate (0, 10, and 20 mM). Error bars are standard deviations from three independent experiments.

fluorescence colonies in the absence of exogenously supplemented 4HB only when harboring the construct pPobR_ubiC-wt (Sensor -Enzyme), confirming that the expression of UbiC resulted in intracellular formation of 4HB, which, in turn, activated the PobR-DM sensor (Supplementary Figure S2). The plasmid containing the sensor alone (pPobR) showed dim colonies in the absence of exogenous 4HB (Figure 3b, Supplementary Figure S2), presumably from low background activity of the native UbiC in *P. putida* KT2440. In the presence of 100 μM 4HB, Sensor and Sensor-Enzyme cells showed relatively similar fluorescence, possibly because of complete inhibition of UbiC by 4HB ($K_i \sim 2\ \mu M$)[12] in the latter, and the observed fluorescence signal was only as a result of sensor activation by exogenous 4HB supplementation in the two cases. Considering the fluorescence reporter is slightly different in the two cases (sfGFP versus sfGFP-UbiC), the fusion protein may reduce the fluorescence intensity resulting in Sensor-Enzyme cells showing marginally weaker intensity than the Sensor-alone cells.

Benzoate is a known inhibitor of UbiC with $K_i > 3$ mM.[12] A ligand docking study covering the complete UbiC protein using the RosettaLigand protocol,[26] predicted positioning of benzoate in the same pocket and orientation as seen in the crystal structure (PDB code 1JD3) and in the lowest energy binding mode in docked 4HB-UbiC complex (Supplementary Figure S3). The docking studies also predicted relatively weaker binding affinity for benzoate compared with 4HB. Hence, when the growth media was supplemented with a high concentration of benzoate (10 mM), the colonies showed diminished fluorescence, confirming inhibition of the UbiC enzyme and reduced production of the 4HB. However, when 100-fold less (100 μM) 4HB was supplemented with 10 mM benzoate, the colonies with either the Sensor or Sensor-Enzyme plasmid showed fluorescence. Together these data indicate that benzoate can inhibit UbiC enzyme activity but does not block the inducer binding pocket of the sensor (Figure 3b).

Mutational Library of UbiC To Reduce Product Inhibition. Based on the product-bound UbiC structure (PDB code 1JD3),[27] amino acid positions that could be mutated to weaken the product binding were determined (Figure 4a). We employed a conservative approach to select residue positions for mutagenesis, since an earlier study showed that even a single mutation in the enzyme was frequently detrimental to its stability.[28] It was also shown in the same study that mutations in the loop (residues 29−34, referred to as the flap) can perturb the product binding to the enzyme. Two mutations L30A and D32A (numbering based on the UbiC structure PDB code 1JD3), were expected to weaken hydrophobic and polar interactions respectively with the rigid portions of the protein. While the two mutations independently reduced product inhibition, the combination of the two failed to show an additive effect in terms of gain-of-functions, probably because of poor stability and low expression of the double mutant protein.[28] We built upon this study and took a two-pronged approach, where, in one case, mutations were further explored in the flap, and in another case, mutations specifically around 4HB were pursued such that product−enzyme interactions are weakened (Figure 4a). For the first set of mutations, we chose to investigate the E31Q and M34V mutations within the flap. E31, a negatively charged amino acid, exhibits a charge interaction with R116 and R126. We hypothesized that a conservative mutation of

DOI: 10.1021/acssynbio.8b00465
ACS Synth. Biol. 2019, 8, 775−786

Table 1. Kinetic Parameters[a] of sfGFP Fused UbiC Variants with a C-Terminal 6×His Tag

UbiC variant	mutations	K_m (μM)	k_{cat} (s^{-1})	k_{cat}/K_m (s^{-1} M^{-1})	K_p (μM)
wild-type	none	32.9 ± 2.8	0.37 ± 0.04	1.1×10^4	2.4 ± 0.2
UbiC-L30A	L30A	74.1 ± 8.7	0.64 ± 0.07	8.6×10^3	13.2 ± 1.0
UbiC-C11	E31Q/I78V/L80V	54.7 ± 3.4	0.51 ± 0.04	9.3×10^3	4.7 ± 0.6
UbiC-C21	M34V/I78V	90.2 ± 7.8	0.67 ± 0.06	7.4×10^3	17.8 ± 1.4
UbiC-C22	E31Q/M34V	147.7 ± 9.4	1.04 ± 0.09	7.0×10^3	19.3 ± 2.5

[a]Mean ± Standard Error from duplicate experiments.

E31 → Q would mitigate that interaction, resulting in an effect similar to the D32A mutation on the same loop that weakens the charge−charge interaction between D32 and R116.[28] Similarly, the effect of the L30A mutation to create a void between position 30 and 34 can be recapitulated by shortening the side chain at position 34 by mutating wild-type methionine to valine.

The other set of mutations focused around the product 4HB in the crystal structure. The R76 → K/M mutations were selected to weaken/disrupt the existing electrostatic interaction between the carboxylate group of 4HB and the arginine at position 76 of the protein. Mutations I78 → V, L80 → V, T92 → A and L114 → V were also selected for diversification of UbiC as these mutations were expected to weaken the 4HB/protein interaction due to shortening of the side chain in each case (Figure 4a). The G90A mutation, as in the product bound structure of UbiC (PDB code 1JD3), is expected to increase the affinity of the 4HB/protein interaction.[27] Hence, we chose the G90 → S mutation since introduction of a hydroxyl group in close proximity of the 4HB aromatic ring was expected to weaken the interaction in addition to causing steric hindrance to 4HB due to a larger side chain. A combinatorial library consisting of the wild-type amino acid and selected conservative mutations at these eight positions in UbiC was created with a theoretical diversity of ∼400, transformed into the *P. putida* strain CJ182, and plated. Transformed colonies (40-fold the library diversity) were scraped and evaluated in subsequent experiments.

Benzoate as a Product Surrogate Molecule for 4HB Sensor-Mediated High-Throughput Screening of UbiC Library for Reduced Product Inhibition. As described in the previous section and in Figure 3, the PobR-based sensor is specific to 4HB, and benzoate fails to activate the sensor. However, UbiC is sensitive to product inhibition from both 4HB (its product) and benzoate (with an affinity 1000-fold weaker than 4HB).[12] These observations were leveraged to relieve the product inhibition of UbiC, where UbiC variants with high activity were selected on the basis of high fluorescence in the presence of the benzoate inhibitor. For selection, a CJ182-based UbiC library was plated in the presence and absence of 10 mM benzoate (Figure 4b). In the absence of any inhibitor (benzoate) or inducer (4HB), the library showed varying fluorescence in the colonies, indicating that the variants were producing 4HB *in vivo* at different levels and inducing the biosensor to express sfGFP in a correlated fashion (Figure 4b, left, Supplementary Figure S4, same plate but under reduced illumination intensity to avoid saturation of the fluorescence). When the library was cultured on 10 mM benzoate with 100 μM 4HB inducer, all of the colonies uniformly accumulated fluorescence (Figure 4b, right), indicating again that the sensor activity is unaffected by the addition of benzoate, as observed above for the wild-type UbiC-sensor strain (Figure 3b). In the presence of 10 mM benzoate inhibitor alone, a small number of colonies were distinctly brighter than the rest, indicating that these colonies were able to make 4HB even in the presence of a high concentration of the benzoate inhibitor (Figure 4b, middle). However, some of the brightest colonies were in a crowded region of the plate. We were concerned that these most crowded regions exhibited higher UbiC activity simply because the local benzoate concentration may have been reduced because of the natural metabolism of benzoate in *P. putida*. Thus, bright colonies from such regions on the plate were not picked. Instead, several *isolated* colonies exhibiting fluorescence above the background from the benzoate-inhibited population were picked and evaluated in liquid culture supplemented with varying concentrations of benzoate. Five mutants of UbiC were identified that exhibited high retention of fluorescence (30−40%) even at 20 mM benzoate (Figure 4c), while the wild-type exhibited very low fluorescence in the cells. The previously published UbiC variant with reduced product inhibition (UbiC-L30A)[28] was grown as a control also showed high retention of cell fluorescence at 20 mM benzoate. Sequencing of the top clones revealed the following mutations: C2: E31Q/T92A; C11: E31Q/I78V/L80V; C14: E31Q/I78V/T92A; C21: M34V/I78V; C22: E31Q/M34V.

Kinetic Analysis of the UbiC Variants. As sfGFP fusions, expression, and yields of the UbiC mutants from single-step affinity purification were comparable with each other (Supplementary Figure S5). We performed an *in vitro* kinetic assessment on a few UbiC variants to understand the mutational effects on the enzymatic parameters (Supplementary Figure S6). As a control for a variant with relieved product inhibition, the previously studied variant UbiC-L30A[28] was also included in the study. Their kinetic parameters, K_m, k_{cat} and K_p, were determined (Table 1). Compared with the wild-type UbiC, the variants, UbiC-C21 and UbiC-C22, showed a 3−5-fold increase in K_m for chorismate along with 7−8-fold increase in product inhibition constant, K_p, confirming that the new variants of UbiC have alleviated product inhibition. The catalytic turnover number, represented by k_{cat}, showed an increase by 2−3-fold in UbiC-C21 and UbiC-C22 compared with the wild-type. Catalytic efficiency (k_{cat}/K_m) of the mutant UbiC variants showed a marginal drop from the wild-type UbiC.

To further assess the role of mutations in the selected UbiC variants, we used the ligand docking protocol in Rosetta[26] to dock the 4HB molecule in the binding pocket of UbiC and calculate the binding energies of different modes and root-mean-square deviation (RMSD) of the atoms from the 4HB position in the crystal structure (PDB code 1JD3). Each docking study showed a dock funnel with minimum energy conformation approaching low RMSD while a subtle difference in the binding energies of 4HB was observed. UbiC-wt showed the tightest binding followed by UbiC-C11 and finally UbiC-C22 and UbiC-C21 that showed similar binding energies

DOI: 10.1021/acssynbio.8b00465
ACS Synth. Biol. 2019, 8, 775−786

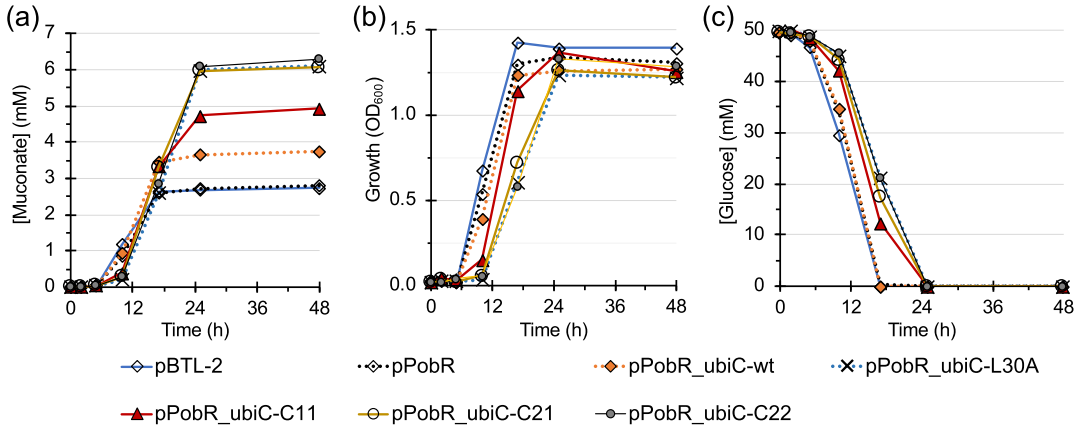

Figure 5. Muconate production and growth for CJ200 *P. putida* strain transformed with pBTL-2 derived plasmids, containing genetic information for the sensor (PobR-DM) and different variants of UbiC enzyme. (a) Muconate production in shake flasks with 50 mM glucose. (b) Growth curves of same strains measured on a plate reader in a 96-well plate. (c) Residual glucose concentration as a function of time in the shake flasks.

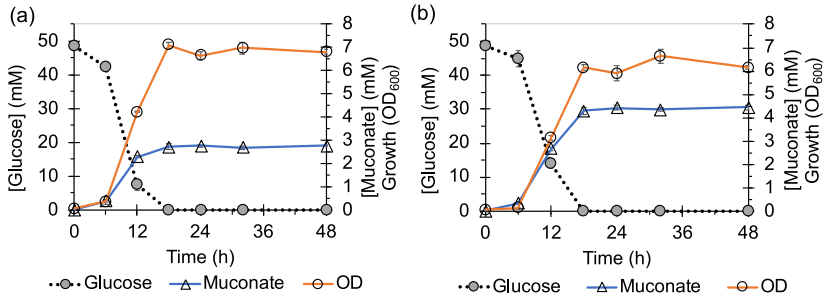

Figure 6. Muconate production in *ubiC* integrated *P. putida* strain CJ200. Growth curve, glucose depletion, and muconate production at 50 mM glucose in (a) CJ200, (b) NP015 where the *ubiC-C22* gene was integrated into the *P. putida* genome. Error bars are standard deviation from triplicate shake flasks.

(Supplementary Figure S7). To further probe the effect of mutations on the "flap", we performed loop modeling within Rosetta[29] to diversify the conformation of the region (residues 29−35) encompassing the "flap". Compared with the wild-type sequence, UbiC-C22 showed a very low energy gap between the two clusters formed by alternate conformations of the loop, suggesting an alternate "open" conformation of the flap was possible due to the mutations E31Q and M34V in UbiC-C22 (Supplementary Figure S8).

UbiC as a Metabolic Shunt for *cis,cis*-Muconic Acid Production in *P. putida*. We next investigated if the UbiC mutants with reduced product inhibition can be applied to enhance the metabolic pathways for biosynthesis of valuable products. To test this, we chose *cis,cis*-muconic acid (muconate) as an end-product as it can be derived from 4HB via the shikimate pathway (Figure 1).[10] We transformed the biosensor/enzyme plasmid with UbiC variants into the *P. putida* strain CJ200, which has been previously engineered to produce muconate.[30] In *P. putida* KT2440, the introduction of the heterologous genes for the DHS dehydratase and protocatechuate (PCA) decarboxylase enables the conversion of dehydroshikimate (DHS) from the shikimate pathway to catechol via PCA. The native catechol-1,2-dioxygenase in the *β*-ketoadipate pathway converts catechol into muconate. Deletion of the downstream genes *catBC* and the regulator encoded by *catR* prevents further metabolism of muconate in the cells. With the introduction of the *E. coli ubiC* gene in CJ200, we introduced a pathway in which UbiC converts chorismate to 4HB, which is then converted to protocatechuate via the native PobA for subsequent conversion to muconate via the pathway described above (Figure 1). We hypothesized that this additional route from the shikimate pathway to muconate might increase the overall flux to this target molecule. Earlier studies showed that in a batch culture with 50 mM glucose as a carbon source, CJ200 produced approximately 2.5 mM of muconate giving a molar yield ([muconate]/[glucose]) of 5%.[30] CJ200 transformed with the pBTL-2 empty vector or the pPobR plasmid (sensor plasmid) and grown in the presence of Kanamycin (50 *μ*g/mL) exhibited a similar yield of ∼5.5% (Figure 5a), indicating that kanamycin and/or the presence of the *sfgfp* gene do not add to any stress or metabolic burden to *P. putida* cells. With the introduction of the wild-type *ubiC* gene using the pPobR_ubiC-wt plasmid expressing sfGFP-fused UbiC under positive feedback regulation (Figure 2c), the muconate yield increased by >30%, giving a final muconate concentration of 3.7 mM (Figure 5a). Moreover, plasmids expressing variants of UbiC with alleviated product inhibition, UbiC-L30A, UbiC-C21, and UbiC-C22, exhibited a final muconate concentration of >6 mM and a yield increase of ∼130% over CJ200 with no heterologous UbiC expression (Figure 5a, Supplementary Figure S5). At 50 mM starting glucose concentration, the UbiC expressing *P. putida* CJ200 strains showed a longer lag phase and slower growth (compare slope of the plot between lag phase and stationary phase), which may be attributed to the metabolic burden caused by diversion of chorismate from the essential pathway toward production of muconate (Figure 5b). As expected, the glucose consumption rates (Figure 5c)

DOI: 10.1021/acssynbio.8b00465
ACS Synth. Biol. 2019, 8, 775−786

correlated well with cell division tracked by optical density, with the fastest growing strains showing the fastest glucose consumption rates.

Genomic Integration of *E. coli ubiC* Gene in *P. putida*. We further investigated the effect of the E31Q/M34V double mutant of UbiC-C22 in the muconate production strain, where the mutant *ubiC* gene was integrated into the genome of *P. putida* CJ200 strain. Simulating the plasmid version of *ubiC-C22* in CJ200, we kept the expression of the UbiC under the positive feedback regulation of PobR and integrated it into the intergenic region between locus tags PP_1642 and PP_1643 to create strain NP015. At 50 mM glucose in a shake flask, CJ200 and NP015 were compared for growth, glucose consumption rates, and muconate production. While the two strains showed comparable rates for glucose consumption and growth, with complete glucose utilization and saturation cell density reached in 18 h, an enhancement in muconate production was observed in NP015 over the parent strain CJ200 (Figure 6). At 18 h, the muconate concentration in the culture media saturated. Muconate concentrations of 2.7 and 4.3 mM were observed in CJ200 and NP015 strains, giving a molar yield of 5.4% and 8.6%, respectively. This gave a yield improvement of 60% in the muconate production strain due to the addition of new carbon flux directed from shikimate pathway toward the heterologous muconate pathway (Figure 6). A small difference in the final OD of the two strains can be attributed to the difference in muconate yields.

DISCUSSION

Advances in synthetic biology tools have enabled the construction of synthetic genetic circuits for a variety of applications. There are many microorganisms that are industrially relevant or metabolically diverse, but they cannot be engineered efficiently due to the lack of synthetic tools to build and evaluate the metabolic efficiency of strains. Hence, a functional 4HB sensor in *P. putida* KT2440 is an addition to the synthetic toolbox that will allow evaluation of multiple genes and pathways leading to the production of 4HB as an intermediate or end product in this critical host. The PobR-DM-based sensor specifically senses 4HB with high sensitivity and contrast ratio, but it insignificantly responds to closely related molecules, such as benzoate or PCA.[14] Thus, the 4HB sensor could also be an important tool in sensing the activity of the aromatic catabolic pathway via *p*-coumarate, a monomeric unit from lignin depolymerization[30] or an intermediate in tyrosine degradation.[31]

To our knowledge, there is no high-throughput, *in vivo* screening approach established for the alleviation of product inhibition in enzymes. Utilizing a sensor-reporter system established in *P. putida*, we were able to screen a library of enzyme variants with a diversity of ∼400 with ease. In this work, we concentrated on a very specific region in the ligand bind pocket of the *E. coli* UbiC and a small flexible region on the protein, called the flap, that shows conformational dynamics using molecular dynamics simulations.[28] Originally, UbiC had been proposed to consist of two relatively large flap regions, residues 21−40 and 97−119, that overlay on the active site.[27] Additionally, the UbiC structure (PDB code 1XLR) also shows multiple ligand binding sites, where a molecule of vanillin is placed in the active site at the same site as 4HB and is more buried while another vanillin molecule is closer to the surface and in close proximity to the L29-M34 flap region.[27] The high-throughput screening setup demonstrated here can be easily extended for a library with a diversity of at least 2 orders of magnitude larger. When coupled with flow cytometry, this technique will be capable of screening even a larger library,[32] allowing exploration of both extended flap regions as well as the secondary ligand binding site simultaneously. This is likely to require substantially less time and effort than *in vitro* screening methods.

It is highly likely that the 4HB (product) binding site in UbiC as observed in the structure (PDB code 1JD3), is also the site for chorismate (substrate) binding. Hence, any mutation that reduces the affinity between 4HB and UbiC is expected to also have a detrimental effect on the substrate-enzyme binding affinity, defined by the enzymatic parameter, K_m. Our double mutants of UbiC (variants C21, C22) as well as the single mutant (UbiC-L30A),[28] all show concerted increase in both K_p and K_m. With the increase in K_p, which means a low residence time of product in the catalytic pocket of the enzyme, the k_{cat} or the turnover number of the enzyme showed an increase by 2- to 3-fold. This resulted in the retention of greater than 60% of the catalytic efficiency in the mutants compared to the wild-type UbiC. Since chorismate is a key hub molecule for a number of pathways, it would be interesting to know the intracellular equilibrium concentration of this important molecule in *P. putida*, and whether the mutant's higher K_m (3−5 fold higher than wild-type) has substantial or negligible effect on the conversion rate and whether a higher turnover rate (2−3 fold higher than wild-type) becomes a key determinant of the conversion efficiency of this route.

UbiC is a key enzyme in the ubiquinone pathway in Gram-negative bacteria. Since *P. putida* KT2440, our host of interest, is also a Gram-negative bacterium, we expect there to be a homologous gene encoding a similar enzyme. The *P. putida* KT2440 genome sequence[33] does contain an annotated *ubiC* gene (locus tag PP_5317, gene id 1042185). The translated sequence of *P. putida ubiC* exhibits a reasonable homology to the *E. coli* UbiC enzyme, with an overall sequence identity of ∼30% as shown by Clustal Omega alignment tool (Supplementary Data 1).[34,35] While regulation of this gene at transcriptional level is worth exploring in *P. putida*, very interestingly, the start codon for *ubiC* translation is "GTG" and not the canonical "ATG". We speculate that the native *ubiC* gene in *P. putida* might be expressed at a low level, which could account for the "dim" (and not completely dark) colonies of *P. putida* transformed with sensor plasmid (Figure 3b, top row, first plate). In the presence of a high concentration of benzoate, an inhibitor of UbiC, the colonies appeared darker (Figure 3b, top row, third plate). A homologous protein sequence search for *E. coli* UbiC using PSI-BLAST+ server[36,37] showed glutamine, though very rare, as an acceptable replacement for E31 (Supplementary Data 2). Similarly, valine for I78 and leucine (though not valine) for M34 were also seen in distant homologues including *P. putida* UbiC (examples shown in Supplementary Data 1 and 2). Our library only had an option of wild-type methionine or valine substitution at position 34, and hence, any functional gain from leucine at this position could not be evaluated in this study. Overall, however, our top variants with reduced product inhibition consist of one or more of these rare natural variations. Thus, UbiC related enzymes may have naturally evolved for enhanced kinetic performance in some species.

DAHP synthase (3-Deoxy-D-arabinoheptulosonate 7-phosphate synthase) catalyzes the first committed step in the

DOI: 10.1021/acssynbio.8b00465
ACS Synth. Biol. 2019, 8, 775−786

Table 2. Strains, Plasmids, and Oligonucleotides Used in This Study

strain	description	reference or source
KT2440	*P. putida* ATCC # 47054	ATCC
CJ182	*P. putida* KT2440 Δ*pobAR*	previous study[25]
CJ200	*P. putida* KT2440 Δ*catRBC*::Ptac:*catA* Δ*pcaHG*::Ptac:*aroY*:*ecdB*:*asbF*	previous study[30]
NP015	*P. putida* KT2440 Δ*catRBC*::Ptac:*catA* Δ*pcaHG*::Ptac:*aroY*:*ecdB*:*asbF*::*pobR-DM-ubiC-C22*	this study
plasmid		
pBTL-2	Kanamycin resistance, pBR322 ori, Plac promoter between soxR and tonB terminators	previous work[24]
pBTL-2_pobR-DM_sfGFP (pPobR)	*pobR-DM,* Pob promoter, *sfgfp* sequences cloned between soxR and tonB terminators	this study
pPobR_ubiC-wt	pPobR with *E. coli ubiC* gene cloned in frame with *sfgfp* using EcoR1/Avr2 sites	this study
pPobR_ubiC-L30A	pPobR with *ubiC* gene containing mutations encoding L30A	this study (L30A mutation)[28]
pPobR_ubiC-C2	pPobR with *ubiC* gene containing mutations encoding E31Q, T92A	this study
pPobR_ubiC-C11	pPobR with *ubiC* gene containing mutations encoding E31Q, I78V, L80V	this study
pPobR_ubiC-C14	pPobR with *ubiC* gene containing mutations encoding E31Q, I78V, T92A	this study
pPobR_ubiC-C21	pPobR with *ubiC* gene containing mutations encoding M34V, I78V	this study
pPobR_ubiC-C22	pPobR with *ubiC* gene containing mutations encoding E31Q, M34V	this study
oligonucleotides		
pBTL2_pobR_overlap_F1	TGCTATGGAGGTCAGGTATGATTTTATACCAGATTGCGCAGTTCG	
PobRpromo_sfGFP_overlap_R1	GTTCTTCTCCTTTGCTAGCCATATGTATATCTCCTTGCTATTTTC	
sfGFP_Fwd	ATGGCTAGCAAAGGAGAAGAAC	
pBTL-2_sfGFP_overlap_Rev	GAGGCTCGTCCTGAATGATATCTTACCTAGGTGTGAATTCAGAAC	
pBTL-2_Fwd	GATATCATTCAGGACGAGCCTCAGACTCC	
pBTL-2_Rev	AATCATACCTGACCTCCATAGCAGAAAGTCAAAAG	
ecUbiC_EcoR1_f	AGTCGAATTCTCACACCCCGCGTTAACGCAAC	
ecUbiC_Avr2_r	AGTCCCTAGGTTAGTACAACGGTGACGCCGG	
ecUbiC_F1	ACAAAACGTTTTGAACAGCAG	
ecUbiC_31_34_R	CTGCTGTTCAAAACGTTTTGTCAYGGAATCCTSCAGCAACAGCCAGTCGAGCAG	
ecUbiC_L30A_R	CTGCTGTTCAAAACGTTTTGTCATGGAATCCTCCGCCAACAGCCAGTCGAGCAG	
ecUbiC_76_78_80_R	GCCACGGTTCACCATCGGCACATAMCAAAAYTTCCHTTAACCAGTAACGAGACTCTTTCG	
ecUbiC_90_92_F	CCGATGGTGAACCGTGGCTTGCCRGTCGTRCCGTCGTTCCTGTGTCAACGTTA	
ecUbiC_114_R	GATGTGAACAGATAGCGTCCTAMCGGCGTTTTACCCAATTTTTG	
ecUbiC_F2	GGACGCTATCTGTTCACATC	
ecUbic_GGlink_6His_Avr2_r	AGTCCCTAGGTTAGTGATGGTGATGGTGATGGCCACCGTACAACGGTGACGCCGG	
F_100up_1642_UbiC	GGCATCATCGCGACGACATCGTCGAAA	
R_100up_1642_UbiC	TATCGAGCTGGCCGGCATGGAGGCG	

shikimate pathway, which results in the production of various aromatic amino acids. Interestingly, all the isozymes of DAHP synthase are feedback inhibited by aromatic amino acids, which functions as a regulatory mechanism to control the carbon input in the shikimate pathway. In CJ200, the single route to muconate introduced by the DHS dehydratase, AsbF, results in a muconate yield of 5% from 50 mM glucose.[30] The addition of another shunt, downstream of the AsbF shunt, which diverts chorismate toward muconate production, showed 60−130% increase in muconate yield depending on whether the *ubiC* gene is genomically integrated or expressed via a plasmid. Even though the second shunt is not as efficient as the first one in terms of carbon conversion since 3 out of 10 carbon atoms (30%) are lost as pyruvate when chorismate is converted into 4HB, we speculate that this route might have an indirect effect on reducing the feedback inhibition of DAHP synthase by the reduced production of aromatic amino acids. Synergistically, such a design has contributed to higher muconate titers.

E. coli UbiC has been used earlier for the production of muconate in *E. coli* with a modest titer,[38] used in conjunction with 3-dehydroshikimate dehydratase as an additional metabolic route to boost the titer of muconate,[10] and explored for sole production of 4HB in *S. cerevisiae*[31] or *P. putida* KT2440.[11] In our study, we developed a method of high-throughput screening against product inhibition in this enzyme, while permitting the enzyme to be tested in the context of the entire cell metabolism. We identified new mutations in UbiC that exhibit enhanced turnover in the enzyme in *in vitro* experiments. At the same time, comparison of the wild-type UbiC and UbiC-C21 or UbiC-C22 (Figure 5a) proved that the mutations were more effective in diverting carbon from the essential shikimate pathway even at physiological concentrations of chorismate (substrate) and 4HB (product). Thus, we have leveraged structure-based protein design and whole-cell high-throughput screening to further advance the synthesis and utilization of 4HB in *P. putida* that can be directly applied to the production of renewable chemicals.

MATERIALS AND METHODS

Growth Medium, Conditions, and Small Molecules. Unless specified, all cultures of *P. putida* were grown in Lysogeny Broth (LB) medium and supplemented with 50 μg/mL kanamycin (Kan_{50}) when necessary to maintain plasmids. LB agar plates were prepared with 1−1.5% agar. The cultures were grown in 14 mL round-bottom culture tubes (BD falcon) in a volume of 3−5 mL, at 30 °C with shaking at 225−250 rpm. 4-HB (Acros), benzoic acid (Fluka), and *cis,cis*-muconic acid (Acros) were prepared as sodium salts by dissolving in an equimolar amount of sodium hydroxide. Hence, the actual

DOI: 10.1021/acssynbio.8b00465
ACS Synth. Biol. 2019, 8, 775−786

forms of 4HB, benzoate, and muconate will be interchangeably used for their respective acid forms.

Plasmids and Strains. Table 2 summarizes the oligonucleotides, plasmids, and strains used in this study. *P. putida* KT2440 (ATCC # 47054) derivatives were used for cloning, for whole-cell biosensing, UbiC library preparation, and screening of various UbiC constructs. *P. putida* KT2440 and the engineered derivative CJ182[25] were used to test the 4HB biosensor construct. CJ182 was used for screening of the UbiC library. *P. putida* KT2440 derivative CJ200[30] was used for the muconate production experiments. The DNA fragment encoding PobR-DM and the native promoter were PCR amplified from an *E. coli* adapted biosensor published earlier[14] using oligonucleotides described in Table 2 that amplified products to include overlap with a broad host range vector backbone and the *sfgfp* gene that encodes the superfolder GFP (sfGFP) reporter. For the backbone, the pBTL-2 vector,[24] a gift from Ryan Gill (Addgene plasmid # 22806), was PCR amplified using the oligonucleotides pBTL-2_Rev and pBTL-2_Fwd (Table 2). The two PCR products along with *sfgfp* gene were assembled using NEBuilder HiFi Assembly kit (New England Biolabs) to create the pBTL-2_PobR-DM_sfGFP plasmid (pPobR). The *E. coli ubiC* gene was PCR amplified from genomic DNA of *E. coli* type B cells (ATCC strain # 11303) using oligonucleotides ecUbiC_EcoR1_f and ecUbiC_Avr2_r (Table 2), and cloned into the pPobR plasmid between *Eco*RI and AvrII sites, such that the *ubiC* gene was in frame with the *sfgfp* gene. The mutation corresponding to the previously published L30A UbiC mutant[28] was introduced by first creating two PCR fragments using oligonucleotides ecUbiC_EcoR1_f and ecUbiC_L30A_R and ecUbiC_F1 and ecUbiC_Avr2_r and the *ubiC* gene as the template and then assembling them with an overlap oligonucleotide method.[39] The mutant gene was cloned into the pPobR as described above. C-terminal 6×His tag versions of the UbiC variants were created using PCR amplification of the gene with oligonucleotides ecUbiC_EcoR1_f and ecUbiC_GGlink_6His_Avr2_r (Table 2). The PCR products were cloned into pPobR in the same way as described earlier. The new gene cassettes encode N-terminal sfGFP-fused UbiC variants with a glycine−glycine linker followed by a 6×His tag in the C-terminus. The electrocompetent cells of *P. putida* were prepared, and transformations were performed according to the established protocol.[40] The pBTL-2-derived plasmids were transformed in *P. putida* strains using electroporation (BioRad) in a 1 mm cuvette at 1.6 kV, 25 μF, and 200 ohms. A typical time constant of 4.7−5.1 ms was observed for a successful transformation. The transformed cells were selected on LB agar plates with Kan_{50}. A small scoop of cells (using 1 μL inoculation loop) from the transformation plates was grown overnight, mixed with glycerol at a final concentration of 20%, and stored in −80 °C as glycerol stocks.

Vector Construction for Genomic Integration. The 5′ and 3′ homology arms flanking the intergenic region between the genes PP_1642 and PP_1643 were PCR amplified from CJ200 strain using KOD Hot Start polymerase (Millipore). The homology arms consisted of 1009 bp of PP_1642 and 947 bp of PP_1643. The *pobR-DM_ubiC-C22* gene cassette was PCR amplified from the pPobR_ubiC-C22 plasmid. The homology arms and the *pobR-DM_ubiC-C22* PCR product were Gibson assembled[41] into the suicide integration vector pk18mobsacB[42−44] using the NEBuilder HiFi Assembly kit (New England Biolabs). This created the pk18mobsacB_ubiC-C22 plasmid with the PobR regulated promoter driving *ubiC-C22* gene expression for genomic integration.

Genomic Integration. Gene integration in the *P. putida* KT2440-derived strain CJ200 was accomplished by electroporation of the pk18mobsacB_ubiC-C22 plasmid as described above. Briefly, chromosomal integration by homologous recombination was selected on LB agar plates supplemented with 100 μg/mL kanamycin. Colonies were then counter-selected for a second crossover event to remove the plasmid from the genome on YT (yeast extract + tryptone) agar plates supplemented with 25% sucrose, as described previously.[42] Insertion was confirmed by PCR amplification using primers (F_100up_1642_UbiC and R_100up_1642_UbiC) that bind outside of the homology regions used to target integration.

Whole Cell Biosensing of 4HB and Benzoate. For 4HB sensing activity of the whole-cell biosensor, a small scoop of pPobR transformed *P. putida* cells from a streaked plate or a glycerol stock was grown overnight as a seed culture. The overnight saturated seed culture was then diluted 100-fold in fresh growth medium, grown for 5−6 h at 30 °C to achieve an OD_{600} of ∼0.6, then distributed in deep 96-well blocks in a volume of 300−500 μL and induced with varying concentrations of 4HB or benzoate. The cultures were grown overnight (14−16 h) under vigorous shaking in a deep-well maximizer shaker (Taitec BioShaker MBR-022UP). The cultures were diluted 100-fold in phosphate-buffered saline (PBS) with 1% sucrose and analyzed using an LSR II flow cytometer (BD Biosciences) or Accuri C6 flow cytometer (BD Biosciences) with standard settings for measurement of GFP fluorescence (ex 488 nm, em ∼530/30 nm). The arithmetic mean fluorescence value of ∼100 000 cells tightly gated based on forward and side scatter (FSC vs SSC) was used for a dose−response plot. The same protocol was followed for comparison of UbiC clones.

Selecting Mutagenesis Sites in UbiC and Library Creation. The UbiC crystal structure with a bound 4HB molecule (PDB code 1JD3)[27] was used for the determination of appropriate sites for mutagenesis that could weaken the 4HB/UbiC interaction. Based on the first shell amino acids (4 Å radius from 4HB ligand atoms), seven positions were identified for mutagenesis in the binding pocket. A few positions on the loop referred to as the flap[28] were also selected for mutagenesis. Mutations were selected such that only small changes in side chain properties (hydrophobic to hydrophobic, charged to polar, polar to hydrophobic or hydrophobic to polar) were achieved. The diversified library of *ubiC* was constructed using the oligonucleotides with wobble at appropriate positions and PCR amplification using *E. coli* genomic DNA containing the *ubiC* gene as a template. The fragments were created using forward and reverse primer pairs of ecUbiC_EcoR1_f and ecUbiC_31_34_R, ecUbiC_F1 and ecUbiC_76_78_80_R, ecUbiC_90_92_F and ecUbiC_114_R, and finally, ecUbiC_F2 and ecUbiC_Avr2_r with the wild-type *ubiC* gene as the template. The fragments were assembled using overlap extension PCR.[39] Complete *ubiC* gene variants were double digested with restriction enzymes *Eco*RI/AvrII restriction endonucleases (NEB Biolabs) and cloned into the pPobR plasmid such that the *ubiC* gene was in the same reading frame as *sfgfp*. The gene library created consisted of zero to eight mutations in any gene, since all the mutations were represented in a small set of random clones as confirmed by Sanger sequencing. Transformation in *P. putida* strain CJ182 was carried out using the electro-

DOI: 10.1021/acssynbio.8b00465
ACS Synth. Biol. 2019, 8, 775−786

poration method as described above. Following transformation, the total number of colonies on the plate representing approximately 40-fold the library diversity were scraped and stored as glycerol stocks. Typical OD_{600} of the glycerol stock was ~1. As needed, a scoop of glycerol stock using 1 μL inoculation loop was sequentially diluted twice in 1 mL of LB to reach approximately 10^4 cells/mL and 100−400 μL of the diluted sample spread on agar plates with suitable growth conditions to get a total of 1000- to 4000-well separated colonies on a 85 mm or 125 mm diameter Petri dish, respectively.

Selection of UbiC Variants with Relieved Product Inhibition. To select clones with relieved product inhibition, *P. putida* cells containing variants of *ubiC* were grown on LB agar plates containing high concentrations (3 and 10 mM) of benzoate. Benzoate works as a proxy for 4HB because the two molecules are aromatic and carry similar charge. Benzoate is capable of inhibiting the enzyme UbiC with a K_p a thousand-fold higher than 4HB,[12] but it does not activate the 4HB biosensor at those concentrations (this work). Colonies were selected visually on the basis of the intensity of their fluorescence using an Illumatool Lighting System (LightTools Research) equipped with a 488 nm excitation filter and photographed using an iPhone 6 or 8 camera through a colored glass filter (515 nm; LightTools Research). Selected colonies were grown and stored as glycerol stocks for later use. The clones were compared in liquid cultures as described above.

Enzyme Expression and Purification. Five-milliliter cultures were grown from the glycerol stocks of *P. putida* CJ182 containing plasmids encoding 6×His tag UbiC variants. At an OD_{600} of ~0.6, the cultures were induced with 1 mM 4HB and further grown for 16 h at 30 °C and 225 rpm shaking. The cultures were centrifuged at 3500*g* for 10 min, and the cell pellets were lysed with 500 μL BugBuster (Novagen) under slow shaking for 30 min. The cell lysates were centrifuged at 15 000*g* for 15 min at 4 °C and the sfGFP-UbiC fusion proteins were purified by Affinity Chromatography using Talon beads (Clontech). For purification, the clarified supernatant for each Ubic variant was mixed with 200 μL of Talon beads in an equilibration buffer (50 mM Tris-HCl, 300 mM NaCl, pH 7.5) for 30 min. The mixture was centrifuged at 2000*g*, the supernatant was discarded, and the pellet consisting of Talon beads with bound protein was washed two times with equilibration buffer containing 50 mM imidazole. Finally, the beads were mixed with elution buffer (50 mM Tris-HCl, 300 mM NaCl, 300 mM Imidazole, pH 7.5) and filtered through a spin column with 0.2 μm filter. The enzyme concentration and purity of the protein in the eluate were determined by absorbance at 280 nm using a Nanodrop (Thermo Scientific) and SDS polyacrylamide gel electrophoresis, respectively.

Determining Enzyme Kinetic Parameters. The production of 4HB from chorismate catalyzed by UbiC is accompanied by release of a pyruvate molecule. Hence, this activity of the purified UbiC proteins was monitored *in vitro* by a second reaction of NADH oxidation at 340 nm during conversion of pyruvate to lactate in a reaction mixture containing 0.5 units of lactate dehydrogenase (Sigma-Aldrich) and 200 μM NADH (Sigma-Aldrich) dissolved in 50 mM Tris-HCl buffer (pH 7.5), 0.5 μg of purified UbiC variants, chorismic acid (Sigma-Aldrich) (30−300 μM), and 4HB (0−200 μM) in a final volume of 100 μL. The reactions were conducted in duplicates in a 96-well plate at 30 °C in the Synergy H4 Hybrid Microplate Reader (Biotek). The kinetic parameters and product inhibition constants were determined as described previously[28] by measuring the initial reaction rates with respect to varying substrate and product concentrations and calculated by fitting the data by nonlinear regression analysis in GraphPad Prism software.

Shake Flask Experiments for Muconate Production. *P. putida* CJ200 transformed with pPobR_ubiC plasmids or with genomically integrated *ubiC-C22* under PobR regulation (NP015) were grown in 125 mL baffled shake flasks containing 25 mL of 1× M9 salts (6.78 g/L Na_2HPO4, 3 g/L KH_2PO4, 0.5 g/L NaCl, 1g/L NH_4Cl), 30−50 mM glucose, 2 mM $MgSO_4$, 100 μM $CaCl_2$, 18 μM $FeSO_4$, and 50 μg/mL kanamycin. Seed cultures were grown from glycerol stocks in LB media supplemented with 50 μg/mL kanamycin, for 16 h, pelleted and washed with M9 growth medium, and subcultured into flasks to a final OD_{600} of 0.05. Cultures were incubated at 30 °C and 225 rpm for up to 2 days. Samples were taken at regular intervals to quantify cell density, glucose consumption, and muconate concentration.

Quantification of Glucose and Muconate Concentrations Using High-Performance Liquid Chromatography (HPLC). To measure muconate concentration, culture samples collected at various time points were centrifuged either at 3500 rpm for 10 min or 16 000 rpm for 1 min. The supernatants were transferred to a 0.22 μm spin column (Corning Costar Spin-X with cellulose acetate membrane), centrifuged, and the filtrates were transferred to HPLC vials for analysis by Agilent 1100 series HPLC system. The samples were analyzed for 10 min on a Fast Acid column [Phenomenex Rezex RFQ-Fast Acid H+ (8%)] using 0.01 N H_2SO_4 at a flow rate of 0.8 mL/min as a mobile phase. A Diode Array Detector (DAD) set at 258 nm wavelength for detection was used for estimating muconate concentration, while a Refractive Index Detector (RID) was used to estimate glucose concentration. Alternatively, the samples were analyzed for 40 min on a SUPELCOGEL H Column (SUPELCO) with 0.1% H_2SO_4 at 0.5 mL/min. The temperature of both column and RID detector were maintained at 45 °C. Glucose and muconate were quantified using RID and peaks were integrated using Agilent Chemstation software. Appropriate standards were made using commercial glucose and muconate samples.

Computational Modeling of UbiC-wt and Mutants. Protein−ligand interaction modeling and sampling of loops for alternate conformations were performed using Rosetta release version 3.10.[45] For all modeling purposes, the structural coordinates of 4HB bound *E. coli* UbiC (PDB code 1JD3) were used. The G90A mutation was reverted back to wild-type glycine using Rosetta fixed backbone design protocol.[46] The structure was further refined using Rosetta relax protocol.[47] The ligands, 4HB, and benzoate were prepared using Avogadro molecular editor and visualization tool (version 1.2.0).[48] The docking studies (global dock) of 4HB and benzoate in relaxed Ubic-wt structure using RosettaLigand protocol[26] was performed in a 22 Å sphere, with center located at the C-gamma atom of L153. A total of 5000 dock trajectories were completed for UbiC-wt and each ligand. Relaxed structural models of UbiC-C11, UbiC-C21, and UbiC-C22 sequences were also generated using the fixed backbone and relax protocols. Local 4HB docking was performed in a 5 Å radius sphere around the native 4HB position in UbiC (PDB code 1JD3). A total of 1000 dock trajectories were performed for each UbiC variant. Ligand binding energy for each docked

DOI: 10.1021/acssynbio.8b00465
ACS Synth. Biol. 2019, 8, 775−786

pose was plotted against the root-mean-square deviation (RMSD) from the native 4HB conformation (both scores calculated by RosettaLigand protocol) to produce dock funnels.

Similarly, a kinematic closure (KIC) protocol[29] was used for modeling of "flap" (residue 29−34 with an added residue 35). The sequence of each UbiC variant was threaded on the 1JD3 structure (A90G/S14F/S81C for UbiC-wt, A90G/S14F/S81C/E31Q/I78V/L80V for UbiC-C11, A90G/S14F/S81C/M34V/I78V for UbiC-C21 and A90G/S14F/S81C/E31Q/M34V for UbiC-C22) using the Rosetta fixed backbone protocol and refined by the relax protocol. Three- and nine-residue fragments for loop modeling were generated from the Robetta server.[49] The KIC protocol performed *de novo* prediction of the specified region (residue 29−35) followed by loop refinement to attain minimum energy conformation. The total score of each model was then plotted against the RMSD of each pose from the input structure.

■ ASSOCIATED CONTENT

Supporting Information

The Supporting Information is available free of charge on the ACS Publications website at DOI: 10.1021/acssynbio.8b00465.

Supporting data, plasmid details, supplementary figures; steps and command lines for computational modeling and data analyses (PDF)

■ AUTHOR INFORMATION

Corresponding Authors

*E-mail: rjha@lanl.gov.
*E-mail: tdale@lanl.gov.

ORCID

Ramesh K. Jha: 0000-0001-5904-3441
Naresh Pandey: 0000-0002-2129-9166
Gregg T. Beckham: 0000-0002-3480-212X

Author Contributions

T.D. and G.B. acquired the funding for the project. C.E.M.S. acquired the funding for preliminary work. R.J. and T.D. planned the research. R.J., N.N, N.P. J.B., and T.K. performed the experiments under the supervision of S.H. and T.D. R.J., S.H., and T.D. analyzed the data. C.J. and G.B. provided microbial engineering expertise and reagents for the experiments. R.J., N.N., C.J., G.B., and T.D. wrote the article with input from everyone.

Notes

The authors declare the following competing financial interest(s): Modified biosensors and biocatalysts and methods of use are subjects of patent applications by Los Alamos National Laboratory.

■ ACKNOWLEDGMENTS

The work was supported by the U.S. Department of Energy (DOE) Energy Efficiency and Renewable Energy Office (EERE) Bioenergy Technologies Office (BETO) for the Agile BioFoundry (to T.D. (under Contract NL0032182) and G.T.B.) and the DOE Science Undergraduate Laboratory Internships (to J.M.B.). Preliminary work was supported by the Defense Threat Reduction Agency (CBCALL12-LS-6-0622 to C.E.M.S.). This research used resources provided by the Los Alamos National Laboratory Institutional Computing Program (under w19_proteng to R.K.J), which is supported by the U.S. Department of Energy National Nuclear Security Administration under Contract No. 89233218CNA000001.

■ REFERENCES

(1) Lynd, L. R., Wyman, C. E., and Gerngross, T. U. (1999) Biocommodity Engineering. *Biotechnol. Prog. 15* (5), 777−793.

(2) Rogers, J. K., Taylor, N. D., and Church, G. M. (2016) Biosensor-Based Engineering of Biosynthetic Pathways. *Curr. Opin. Biotechnol. 42*, 84−91.

(3) Harrington, L. B., Jha, R. K., Kern, T. L., Schmidt, E. N., Canales, G. M., Finney, K. B., Koppisch, A. T., Strauss, C. E. M., and Fox, D. T. (2017) Rapid Thermostabilization of *Bacillus Thuringiensis* Serovar Konkukian 97−27 Dehydroshikimate Dehydratase through a Structure-Based Enzyme Design and Whole Cell Activity Assay. *ACS Synth. Biol. 6* (1), 120−129.

(4) Tang, S.-Y., Qian, S., Akinterinwa, O., Frei, C. S., Gredell, J. A., and Cirino, P. C. (2013) Screening for Enhanced Triacetic Acid Lactone Production by Recombinant *Escherichia Coli* Expressing a Designed Triacetic Acid Lactone Reporter. *J. Am. Chem. Soc. 135* (27), 10099−10103.

(5) Yang, P., Wang, J., Pang, Q., Zhang, F., Wang, J., Wang, Q., and Qi, Q. (2017) Pathway Optimization and Key Enzyme Evolution of N -Acetylneuraminate Biosynthesis Using an in Vivo Aptazyme-Based Biosensor. *Metab. Eng. 43*, 21−28.

(6) Rogers, J. K., and Church, G. M. (2016) Genetically Encoded Sensors Enable Real-Time Observation of Metabolite Production. *Proc. Natl. Acad. Sci. U. S. A. 113* (9), 2388−2393.

(7) Binder, S., Siedler, S., Marienhagen, J., Bott, M., and Eggeling, L. (2013) Recombineering in *Corynebacterium Glutamicum* Combined with Optical Nanosensors: A General Strategy for Fast Producer Strain Generation. *Nucleic Acids Res. 41* (12), 6360−6369.

(8) Lehning, C. E., Siedler, S., Ellabaan, M. M. H., and Sommer, M. O. A. (2017) Assessing Glycolytic Flux Alterations Resulting from Genetic Perturbations in *E. Coli* Using a Biosensor. *Metab. Eng. 42*, 194−202.

(9) Mahr, R., Gätgens, C., Gätgens, J., Polen, T., Kalinowski, J., and Frunzke, J. (2015) Biosensor-Driven Adaptive Laboratory Evolution of l -Valine Production in *Corynebacterium Glutamicum*. *Metab. Eng. 32*, 184−194.

(10) Thompson, B., Pugh, S., Machas, M., and Nielsen, D. R. (2018) Muconic Acid Production via Alternative Pathways and a Synthetic "Metabolic Funnel". *ACS Synth. Biol. 7* (2), 565−575.

(11) Yu, S., Plan, M. R., Winter, G., and Krömer, J. O. Metabolic Engineering of *Pseudomonas Putida* KT2440 for the Production of Para-Hydroxy Benzoic Acid. *Front. Bioeng. Biotechnol.* 2016, *4*, DOI: 10.3389/fbioe.2016.00090.

(12) Holden, M. J., Mayhew, M. P., Gallagher, D. T., and Vilker, V. L. (2002) Chorismate Lyase: Kinetics and Engineering for Stability. *Biochim. Biophys. Acta, Protein Struct. Mol. Enzymol. 1594* (1), 160−167.

(13) Nichols, B. P., and Green, J. M. (1992) Cloning and Sequencing of *Escherichia Coli* UbiC and Purification of Chorismate Lyase. *J. Bacteriol. 174* (16), 5309−5316.

(14) Jha, R. K., Chakraborti, S., Kern, T. L., Fox, D. T., and Strauss, C. E. M. (2015) Rosetta Comparative Modeling for Library Design: Engineering Alternative Inducer Specificity in a Transcription Factor. *Proteins: Struct., Funct., Genet. 83* (7), 1327−1340.

(15) Draths, K. M., and Frost, J. W. (1994) Environmentally Compatible Synthesis of Adipic Acid from D-Glucose. *J. Am. Chem. Soc. 116* (1), 399−400.

(16) Vardon, D. R., Rorrer, N. A., Salvachúa, D., Settle, A. E., Johnson, C. W., Menart, M. J., Cleveland, N. S., Ciesielski, P. N., Steirer, K. X., Dorgan, J. R., and Beckham, G. T. (2016) Cis, Cis -Muconic Acid: Separation and Catalysis to Bio-Adipic Acid for Nylon-6,6 Polymerization. *Green Chem. 18* (11), 3397−3413.

(17) Suastegui, M., Matthiesen, J. E., Carraher, J. M., Hernandez, N., Rodriguez Quiroz, N., Okerlund, A., Cochran, E. W., Shao, Z., and

DOI: 10.1021/acssynbio.8b00465
ACS Synth. Biol. 2019, 8, 775−786

Tessonnier, J.-P. (2016) Combining Metabolic Engineering and Electrocatalysis: Application to the Production of Polyamides from Sugar. *Angew. Chem., Int. Ed. 55* (7), 2368−2373.
(18) Vardon, D. R., Franden, M. A., Johnson, C. W., Karp, E. M., Guarnieri, M. T., Linger, J. G., Salm, M. J., Strathmann, T. J., and Beckham, G. T. (2015) Adipic Acid Production from Lignin. *Energy Environ. Sci. 8* (2), 617−628.
(19) Lu, R., Lu, F., Chen, J., Yu, W., Huang, Q., Zhang, J., and Xu, J. (2016) Production of Diethyl Terephthalate from Biomass-Derived Muconic Acid. *Angew. Chem. 128* (1), 257−261.
(20) Rorrer, N. A., Vardon, D. R., Dorgan, J. R., Gjersing, E. J., and Beckham, G. T. (2017) Biomass-Derived Monomers for Performance-Differentiated Fiber Reinforced Polymer Composites. *Green Chem. 19* (12), 2812−2825.
(21) Rorrer, N. A., Dorgan, J. R., Vardon, D. R., Martinez, C. R., Yang, Y., and Beckham, G. T. (2016) Renewable Unsaturated Polyesters from Muconic Acid. *ACS Sustainable Chem. Eng. 4* (12), 6867−6876.
(22) Jha, R. K., Kern, T. L., Kim, Y., Tesar, C., Jedrzejczak, R., Joachimiak, A., and Strauss, C. E. M. (2016) A Microbial Sensor for Organophosphate Hydrolysis Exploiting an Engineered Specificity Switch in a Transcription Factor. *Nucleic Acids Res. 44* (17), 8490−8500.
(23) Pédelacq, J.-D., Cabantous, S., Tran, T., Terwilliger, T. C., and Waldo, G. S. (2006) Engineering and Characterization of a Superfolder Green Fluorescent Protein. *Nat. Biotechnol. 24* (1), 79−88.
(24) Lynch, M. D., and Gill, R. T. (2006) Broad Host Range Vectors for Stable Genomic Library Construction. *Biotechnol. Bioeng. 94* (1), 151−158.
(25) Jha, R. K., Bingen, J. M., Johnson, C. W., Kern, T. L., Khanna, P., Trettel, D. S., Strauss, C. E. M., Beckham, G. T., and Dale, T. (2018) A Protocatechuate Biosensor for *Pseudomonas Putida* KT2440 via Promoter and Protein Evolution. *Metab. Eng. Commun. 6*, 33−38.
(26) Davis, I. W., and Baker, D. (2009) RosettaLigand Docking with Full Ligand and Receptor Flexibility. *J. Mol. Biol. 385* (2), 381−392.
(27) Smith, N., Roitberg, A. E., Rivera, E., Howard, A., Holden, M. J., Mayhew, M., Kaistha, S., and Gallagher, D. T. (2006) Structural Analysis of Ligand Binding and Catalysis in Chorismate Lyase. *Arch. Biochem. Biophys. 445* (1), 72−80.
(28) Han, S.-S., Kyeong, H.-H., Choi, J. M., Sohn, Y.-K., Lee, J.-H., and Kim, H.-S. (2016) Engineering of the Conformational Dynamics of an Enzyme for Relieving the Product Inhibition. *ACS Catal. 6* (12), 8440−8445.
(29) Mandell, D. J., Coutsias, E. A., and Kortemme, T. (2009) Sub-Angstrom Accuracy in Protein Loop Reconstruction by Robotics-Inspired Conformational Sampling. *Nat. Methods 6* (8), 551−552.
(30) Johnson, C. W., Salvachúa, D., Khanna, P., Smith, H., Peterson, D. J., and Beckham, G. T. (2016) Enhancing Muconic Acid Production from Glucose and Lignin-Derived Aromatic Compounds via Increased Protocatechuate Decarboxylase Activity. *Metab. Eng. Commun. 3*, 111−119.
(31) Krömer, J. O., Nunez-Bernal, D., Averesch, N. J. H., Hampe, J., Varela, J., and Varela, C. (2013) Production of Aromatics in *Saccharomyces Cerevisiae*—A Feasibility Study. *J. Biotechnol. 163* (2), 184−193.
(32) Jha, R. K., Kern, T. L., Fox, D. T., and Strauss, C. E. M. (2014) Engineering an Acinetobacter Regulon for Biosensing and High-Throughput Enzyme Screening in *E. Coli* via Flow Cytometry. *Nucleic Acids Res. 42* (12), 8150−8160.
(33) Belda, E., van Heck, R. G. A., José Lopez-Sanchez, M., Cruveiller, S., Barbe, V., Fraser, C., Klenk, H.-P., Petersen, J., Morgat, A., Nikel, P. I., et al. (2016) The Revisited Genome of Pseudomonas Putida KT2440 Enlightens Its Value as a Robust Metabolic Chassis. *Environ. Microbiol. 18* (10), 3403−3424.
(34) Sievers, F., Wilm, A., Dineen, D., Gibson, T. J., Karplus, K., Li, W., Lopez, R., McWilliam, H., Remmert, M., Söding, J., et al. (2011) Fast, Scalable Generation of High-Quality Protein Multiple Sequence Alignments Using Clustal Omega. *Mol. Syst. Biol. 7*, 539−539.
(35) McWilliam, H., Li, W., Uludag, M., Squizzato, S., Park, Y. M., Buso, N., Cowley, A. P., and Lopez, R. (2013) Analysis Tool Web Services from the EMBL-EBI. *Nucleic Acids Res. 41* (W1), W597−W600.
(36) Zimmermann, L., Stephens, A., Nam, S.-Z., Rau, D., Kübler, J., Lozajic, M., Gabler, F., Söding, J., Lupas, A. N., and Alva, V. (2018) A Completely Reimplemented MPI Bioinformatics Toolkit with a New HHpred Server at Its Core. *J. Mol. Biol. 430* (15), 2237−2243.
(37) Camacho, C., Coulouris, G., Avagyan, V., Ma, N., Papadopoulos, J., Bealer, K., and Madden, T. L. (2009) BLAST+: Architecture and Applications. *BMC Bioinf. 10* (1), 421.
(38) Sengupta, S., Jonnalagadda, S., Goonewardena, L., and Juturu, V. (2015) Metabolic Engineering of a Novel Muconic Acid Biosynthesis Pathway via 4-Hydroxybenzoic Acid in *Escherichia Coli*. *Appl. Environ. Microbiol. 81* (23), 8037−8043.
(39) Horton, R. M., Cai, Z. L., Ho, S. N., and Pease, L. R. (2013) Gene Splicing by Overlap Extension: Tailor-Made Genes Using the Polymerase Chain Reaction. *BioTechniques 54* (3), 528−535.
(40) Choi, K.-H., Kumar, A., and Schweizer, H. P. (2006) A 10-min Method for Preparation of Highly Electrocompetent *Pseudomonas Aeruginosa* Cells: Application for DNA Fragment Transfer between Chromosomes and Plasmid Transformation. *J. Microbiol. Methods 64* (3), 391−397.
(41) Merryman, C., and Gibson, D. G. (2012) Methods and Applications for Assembling Large DNA Constructs. *Metab. Eng. 14* (3), 196−204.
(42) Johnson, C. W., and Beckham, G. T. (2015) Aromatic Catabolic Pathway Selection for Optimal Production of Pyruvate and Lactate from Lignin. *Metab. Eng. 28*, 240−247.
(43) Marx, C. J. (2008) Development of a Broad-Host-Range SacB-Based Vector for Unmarked Allelic Exchange. *BMC Res. Notes 1*, 1.
(44) Schäfer, A., Tauch, A., Jäger, W., Kalinowski, J., Thierbach, G., and Pühler, A. (1994) Small Mobilizable Multi-Purpose Cloning Vectors Derived from the *Escherichia Coli* Plasmids PK18 and PK19: Selection of Defined Deletions in the Chromosome of *Corynebacterium Glutamicum*. *Gene 145* (1), 69−73.
(45) Leaver-Fay, A., Tyka, M., Lewis, S. M., Lange, O. F., Thompson, J., Jacak, R., Kaufman, K., Renfrew, P. D., Smith, C. A., Sheffler, W., et al. (2011) Rosetta3: An Object-Oriented Software Suite for the Simulation and Design of Macromolecules. *Methods Enzymol. 487*, 545−574.
(46) Leaver-Fay, A., Snoeyink, J., and Kuhlman, B. On-the-Fly Rotamer Pair Energy Evaluation in Protein Design. In *Bioinformatics Research and Applications*; Măndoiu, I., Sunderraman, R., and Zelikovsky, A., Eds.; Lecture Notes in Computer Science; Springer: Berlin, 2008; pp 343−354.
(47) Tyka, M. D., Keedy, D. A., André, I., DiMaio, F., Song, Y., Richardson, D. C., Richardson, J. S., and Baker, D. (2011) Alternate States of Proteins Revealed by Detailed Energy Landscape Mapping. *J. Mol. Biol. 405* (2), 607−618.
(48) Hanwell, M. D., Curtis, D. E., Lonie, D. C., Vandermeersch, T., Zurek, E., and Hutchison, G. R. (2012) Avogadro: An Advanced Semantic Chemical Editor, Visualization, and Analysis Platform. *J. Cheminf. 4* (1), 17.
(49) Kim, D. E., Chivian, D., and Baker, D. (2004) Protein Structure Prediction and Analysis Using the Robetta Server. *Nucleic Acids Res. 32*, W526−W531.

DOI: 10.1021/acssynbio.8b00465
ACS Synth. Biol. 2019, 8, 775−786